Spiking Neural Network Models for the Emergence of Patterned Activity in Grid Cell Populations

Gwendolyn English

Advisor: Dr. Yulia Sandamirskaya
Prof. Dr. M. Fatih Yanick

Institute of Neuroinformatics
ETH Zurich & University of Zurich

This dissertation is submitted for the degree of
Master of Science

20th September 2017

Abstract

The periodic firing fields of grid cells constitute an internally generated representation of physical space. Since their discovery in 2005, several classes of computational models have aimed to reproduce the spatially periodic grid cell fields. However, current models are often founded upon reduced dynamics not representative of the biological networks in which grid cells are commonly found. In this thesis, we present a novel formulation of a continuous attractor model of grid cells characteristic of the actual connectivity found within medial entorhinal cortex layer II. With an explicit representation of both the principal excitatory cells and inhibitory interneurons, and their disynaptic connections, our network model provides better insights into the temporal and spatial stability of the underlying continuous attractor dynamics. Additionally, the representation of both excitatory and inhibitory populations enables the introduction of biologically plausible plasticity rules that are used to evaluate the stability of the network dynamics. Our results indicate that a plasticity-enabled network is temporally stable and that simple spike-timing dependent plasticity rules are capable of refining the behavior of an initially imprecise network structure. These findings may be critical for understanding the development of grid cell networks during early postnatal life.

Table of contents

List of Figures

List of Tables

I

Introduction

Chapter 1

Biological Properties of Grid Cells and Their Role in Spatial Representation

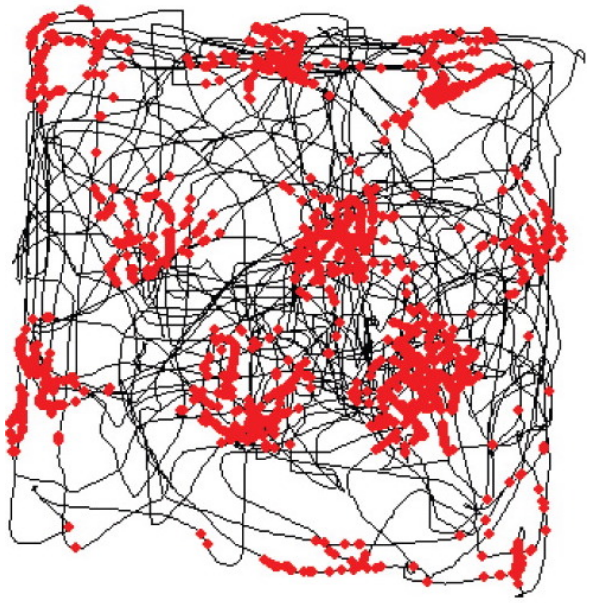

Fig. 1.1 The firing locations of a single grid cell overlaid onto the animal trajectory. The receptive fields of the grid cell create a hexagonal pattern of activity that tessalates the entire space [1].

In 2004 researchers in Trondheim, Norway led by May-Britt and Edvard Moser first reported the existence of neurons with receptive fields that periodically tiled the surface of an environment upon which rats navigated [2]. Figure 1 depicts one such of these neurons, where the solid black line indicates the trajectory of the rat and the red dots indicate the location in which the individual neuron fired. The team of researchers in Norway named these neurons *grid cells*, the properties of which have sparked a wealth of experimental, theoretical and computational research aimed at elucidating their utility and genesis.

1.1 A Primer on Grid Cells

While recording cells in the medial entorhinal cortex (MEC) of rats as they freely navigated an arena, researchers identified that a selection of the recorded neurons fired at spatially relevant positions of the rat's trajectory [2]. Specifically, a grid cell would fire anytime the rat navigated over the corner of equilateral triangles that tiled the entire arena space. While such grid cells have been discovered in other nearby brain regions such as the pre- and parasubiculum, the highest density of these cells has been found to reside within MEC layer II (MEC LII), which account for approximately 50% of all recorded cells [3] [4]. Stellate cells are the primary principal cell type in MEC LII, accounting for 67% of all principal cells, and in vivo recordings suggest that they are the cells most frequently identified as grid cells [5].

Although grid cells appear to directly represent elements of physical space, their specific purpose in navigation has yet to be established. In conjunction with several other spatial representation cell types, grid cells have been proposed to participate in an agent's internal representation of the world [6]. Specifically, researchers have proposed that grid cells could be used to complete path integration between two recently visited locations in space or that they may be used for vector navigation to specifically plan a path to a novel, desired location [7] [8]. While this thesis will focus on the network properties capable of producing a collection of grid cells rather than their specific contribution to navigation, a review of other known spatial representation cell types provides a richer framework with which to understand the origin of the brain's internal representation of the physical world.

1.2 Other Spatial Representation Cells in the Hippocampal Formation

In addition to grid cells, a variety of other neurons exhibiting spatial representation qualities have been identified in the hippocampal formation. An understanding of all of these spatially tuned neurons is critical for garnering insight into the emergence of grid cells.

The *hippocampal formation*, namely the hippocampus, subiculum, and the entorhinal cortices, was first implicated for encoding a representation of physical space in 1971 with the discovery of place cells [9]. Since then, many additional spatial representation cell types have been discovered in this region, among them, grid cells, head direction cells, speed cells, and border cells. This section will contain a description of the aforementioned cell types found in the hippocampal formation, with an emphasis on the experimental findings of their functional and structural interactions with grid cells. It should be noted that what follows does not represent a comprehensive list of all of the spatial representation cells that have thus far been identified, however these cells types have implications on the computational model described in the following chapters.

1.2.1 Place Cells

Place cells are described as cells whose firing rates are maximal when an agent is in a specific location in an environment [10]. They are found in largest quantity in the Cornu Ammonis (CA) regions of

the hippocampus, specifically in CA1 and CA3. These populations of unique place cells together compose a representation of all positions in any given environment.

Since their discovery, several publications have reported on the possible functional interaction between place cells and grid cells. Most commonly, it has been suggested that the unique receptive fields of place cells could be generated by a combination of periodic grid fields [11]. While there yet remains no direct experimental evidence for this grid cell-to-place cell functional interaction, a study published in 2013 indicated that the presence of stable grid cells in MEC LII required the external excitatory drive that the hippocampus provides via backprojections to this region [12]. As the hippocampal regions projecting towards MEC LII are abundant with place cells, it is possible that the specific properties of place cells functionally contribute to grid cell firing.

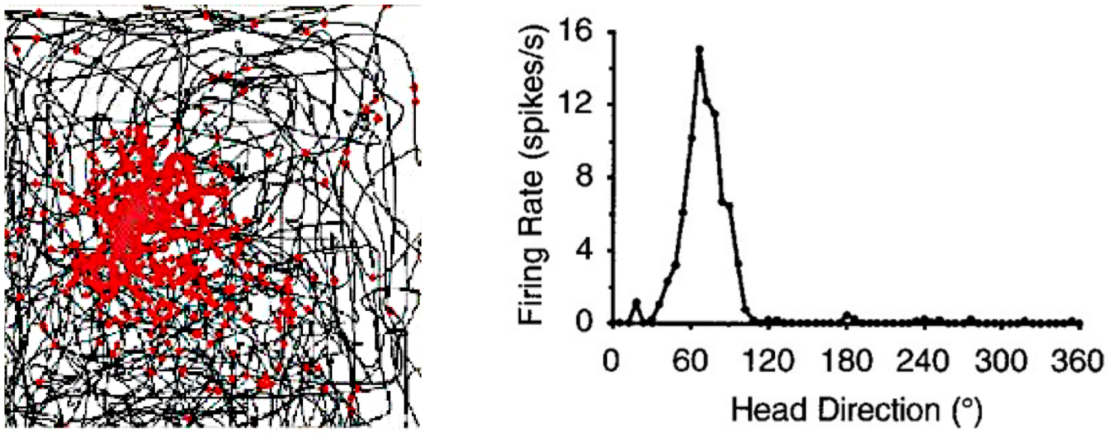

Fig. 1.2 Behavior of a place cell and head direction cell adapted from [13] and [14]. Place cells uniquely encode a specific location or locations in any given space while head direction cells encode the orientation of an agent within a space.

1.2.2 Head Direction Cells

Following the discovery of place cells, Ranck and colleagues reported in 1984 on the existence of a new spatial representation cell type in the pre- and post-subiculum of rats, namely *head direction cells* [15] [16]. Their study uncovered neurons whose firing rates corresponded to the directionality of the rat's head along the horizontal plane, regardless of location, with maximal firing within only a small arc of space. Interestingly, head direction cells maintain their receptive fields also during navigation in darkness, indicating that they could be driven by a self-motion representation. These cells have since been discovered dispersely both within and outside of the hippocampal formation, with presence in the MEC, posterior cortex, anterior thalamic nuclei, and retrospenial cotex [17] [18] [19] [20]. As head direction cells can be found co-located with grid cells in MEC LII, there exists the potential that these two spatial representation cell types may have a functional interaction. A first indication that head direction cells may contribute to grid cell firing fields was reported in the same study that

indicated that hippocampal input was necessary to maintain the spatial periodicity of grid cells; when the hippocampal drive was removed, grid cells started to develop a tuning towards heading direction [12].

1.2.3 Border Cells

Several decades after the discovery of place cells and head direction cells, the same research team responsible for identifying grid cells unearthed yet another spatial representation neuron in 2008, the *border cell*. Intermingled among the grid cells in MEC LII and otherwise found dispersely thoughout all layers of MEC and the parasubiculum, border cells display a proclivity to fire whenever an agent is proximal to an environmental boundary [21]. This particular cell type accounts for approximately 10% of all sampled neurons within MEC and may therefore also have a functional interaction with the populous grid cells found within the same region.

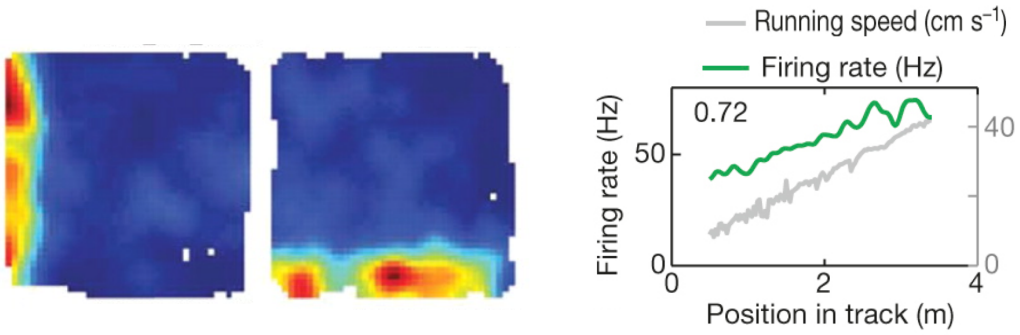

Fig. 1.3 Behavior of border cells and speed cell adapted from [21] and [22]. Border cells have receptive fields along spatial boundaries while speed cells exhibit firing rates that linearly correspond with agent speed.

1.2.4 Speed Cells

Most recently, in 2015 *speed cells* were identified as having firing rates that correspond with nearly instantaneous running speed [22]. While speed cells do not directly map a feature of physical space, they do represent an aspect of an agent's motion throughout that space. Like head direction cells and border cells, they are also found intermingled within grid cells in MEC LII, and have also been identified throughout all other layers of MEC with a near uniform presence of approximately 15% in each layer [22]. The identified speed cells exhibited increases in firing rate with linear response to increased agent speed. Notably, like grid cells, speed cells also display a slightly prospective representation of motion, namely that both cell types fire in accordance with an agent's future speed or location, both specifically 50 - 80 ms advanced [22]. The co-location and shared prospective bias of both grid cells and speed cells allows for the possible interaction of the two classes of neurons.

1.3 Development of Grid Cells

Following the identification of such a wealth of spatial representation cells in the hippocampal formation, researchers began to conduct experiments to elucidate the structural and functional maturation of these neurons during early post-natal development. Results of these developmental experiments published over the past decade have begun to illuminate both how and when the stereotyped firing patters of spatial representation cells emerge during the first weeks and months of motion.

1.3.1 Functional Maturation of Spatial Representation Cell Types in the Hippocampal Formation

In 2010, two different research groups first reported on the functional development of various spatial representation cell types in the early postnatal development of rats [23] [24]. While their publications provided a similar account of the early behavior of place cells and head direction cells, they also contained somewhat contradictory reports about the functional development of grid cells. Both the teams of researchers in London and in Trondheim identified that head direction cells exhibited stable, adult-like firing behavior during the young rat pup's first exploration outside of the nest, occurring around postnatal day 16 (P16) [23] [24]. Similarly, place cells were identified by both groups as having a somewhat slower developmental time course, namely that they were in fact present in small quantities during the first navigation away from the nest however that the number and stability of place cells increased over time during the first four weeks of life [23] [24].

With respect to the development of grid cells, the two studies published in 2010 contained different reports of the first emergence of grid cells and of the time course of their refinement. Langston and colleagues reported that grid cells were recorded on the rat pup's first departure from the nest on P16, but also noted that the refinement of the periodic properties of the early measured grid cells, as well as the overall increase in abundance of grid cells within MEC LII, occurred over a more protracted time period, namely from P16-P34 [23]. In contrast to the reports from Trondheim, Wills and colleagues noted that grid cells were not yet present during the first moments of exploration, rather that they appeared after approximately four days of exploration on P20 and that they subsequently underwent a rapid development towards adult like firing pattern stability over the following two days, achieving steadily high grid scores by P22 [24]. These increased grid scores, which represent the degree of rotational symmetry of a grid cell's hexagonal firing fields, indicate that the cell stably produced a periodic representation of space. A later study by Wills et al reported rather that the emergence of grid cells in MEC was marked by abrupt, adult like firing patterns at P19, opening the question of what network mechanisms may generate a near immediate appearance of cells with such a stereotyped relationship with physical space [25].

To date, no studies have been published regarding the time course of development of either border or speed cells.

1.3.2 Structural Maturation of Cells along the Entorhinal- Hippocampal Circuit

In addition to investigating the functional maturation of the spatial representation cells in the hippocampal formation, it is of value to review the early postnatal structural development of cells along the entorhinal-hippocampal circuit. In early 2017, researchers in Norway reported the results of their investigation of the increase in maturational markers found along this circuit in mice [26].

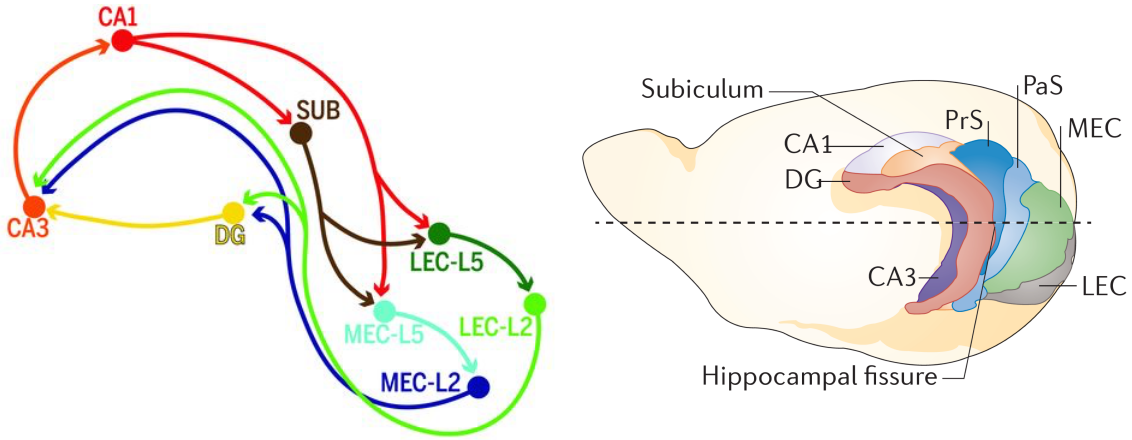

Fig. 1.4 The entorhinal-hippocampal circuit explored in Donato et al [26]. MEC layers II and V (MEC-L2, MEC-L5), the dentate gyrus (DG), cornu ammonis regions (CA1, CA3) and the subiculum (SUB) are depicted. Within these regions are found a vast number of spatial representation cells with the greatest density of grid cells found in MEC-L2. While previous publications have reported on the functional maturation of spatial representation cells, this work lends insight into the possible structural interactions and maturation in the regions giving rise to these cells. A developmental theory of grid cells should be compatible with both the functional and structural maturation studies. On the right is a depiction of the hippocampal formation in the rat brain. The protruding region on the left is the olfactory bulb, and the hippocampal formation is located in the posterior region of the brain. Image taken from Moser et al [27].

Figure 1.2 displays the circuit Donato and colleagues investigated, with the various parts of the entorhinal-hippocampal circuit represented: medial entorhinal cortices layers II and V (MEC-L2, MEC-L5), lateral entorhinal cotrices layers II and V (LEC-L2, LEC-L5), dentate gyrus (DG), cornu ammonis regions I and III (CA1, CA3) and the subiculum (SUB). As with the functional development studies published in 2010, their investigations focused on the second to fourth week of postnatal life and reported on the increased expression of maturational markers along the circuit and how manipulation of activity in the circuit affected the development of downstream regions. Understanding how early activity within the circuit affected structural development may lend insights into the functional interations between different spatial representation cells, such as grid cells and speed cells in MEC LII, place cells in hippocampal regions CA1 and CA3. Additionally, any developmental theory of grid cell networks should be compatible with the time course of the structural maturation of the hippocampal formation in early postnatal life.

The publication contained a number of important findings directly relevant to the development of grid cells and the circuit along which they reside. Notably, the research team reported that the upregulation of expression of maturational markers followed a stage-wise progression that began with stellate cells in MEC LII and moved linearly along the downstream regions within the circuit. They also noted that excitatory activity in each layer of the circuit was necessary for structural maturation to occur in subsequent areas, the process of which began with the maturation and activity of stellate cells in MEC LII [26]. Finally, it was reported that the stellate cells in MEC LII were not reliant on upstream excitatory activity in order for maturation to progress, rather the stellate cells matured in the absence of projected activity in accordance with their cellular birthdate. Unlike the other cell types in MEC LII, stellate cells were discovered to be arranged along the dorsoventral axis in accordance with their birthdate, with earlier born cells clustered together more dorsally and later born cells grouped in ventral regions.

As previously noted, grid cells account for the majority of stellate cells in MEC LII [5]. Findings from Donato's 2017 study seem to implicate that these stellate cells are critical for the maturation of the other cells, such as inhibitory interneurons, in MEC LII as well as cells located downstream in the entorhinal-hippocampal circuit. Given both the functional development findings from 2010 and the structural development findings from 2017, how might a network structure capable of producing grid cells be formed and quickly refined?

1.3.3 Developmental Hypothesis

There are two primary categories of network models capable of generating cells that produce the periodic responses observed from cells that reside with MEC LII, namely *oscillatory-interference* models and *continuous attractor* models [28] [29] [30] [31]. Models in both of these categories describe the connectivity of a stable, adult network that is capable of replicating the responses of grid cells. The oscillatory-interference model generates grid cell firing activity through the interference of constant background theta oscillations and specially spaced, velocity-dependent theta oscillations. Models of the continuous attractor type instead rely on a network of recurrently connected neurons with a specially shifted connection scheme. After the publication of the these two theoretical models, several experimental studies have reported findings that contradict the conclusions of the oscillatory-interference model hypothesis [32] [33] [34] [35]. The presence of grid cells in animals that do not exhibit the theta oscillations required by the oscillatory-interference model, and the lack of theta-modulated firing rates predicted in grid cells generated by the model, represent significant gaps in the theory underlying this model class. In contrast, recent studies have linked experimental findings to properties consistent with the continuous attractor model hypothesis [5] [36] [12] [37]. The underlying synaptic connectivity found within MEC LII, as well as the coordinated behavior between multiple grid cells produced when a strong excitatory feedforward drive is present, are all findings supportive of the dynamics of the continuous attractor models.

While continuous attractor network models of grid cells account for the observed, stable spatially periodic firing patterns of cells recorded from the adult MEC LII, the experimental findings of the functional and structural development publications described in the previous section would suggest that any such network mechanism would not be entirely hardwired. Although the two functional development studies from 2010 indicate different time courses for maturation of grid cell firing stability, both specify that grid cells increase in their periodic regularity over the first days of exploration and after other spatial representation cell types begin to also mature.

Despite the gap in understanding the rapid emergence of a stable grid cell network, few models have been proposed that could account for the emanation of the network connectivity required to produce spatially periodic responses. In 2008, Kropff and Treves proposed a developmental model that enabled the emergence of individual grid cells via the introduction of plasticity combined with adaptation [38]. While this model accounted for the grid cells from their inception, it did not result in a network of grid cells that matches the actual connectivity observed within MEC LII [5]. Several years later in 2014, Widloski and Fiete proposed a developmental model of grid cells that depended on plasticity between several populations of recurrently connected cells and considerable experience to generate neurons with spatially periodic responses [39]. Though this developmental model produced a network that exhibited continuous attractor dynamics and aligned with the observed connectivity in MEC LII, it relied on several substantial assumptions. Notably, in order for the grid cell network to develop, the model required the presence of a fully developed network of place cells that evenly tiled the exploration space, neither of which align with the findings of early postnatal or adult place cell networks. Additionally, before the emergence of any grid cells within the model, the agent needed to spend significant amounts of time exploring all regions of available space, another feature that is not in agreement with experimental findings.

As the current literature still does not account for the observed development of stable grid cells in early postnatal life, we explore mechanisms that illuminate the processes underlying the early formation of a continuous attractor network of grid cells. In contrast to current developmental models, we seek a network structure consistent with continuous attractor dynamics that exhibits grid cells whose spatial stability quickly increases with only limited experience. Given the observed rapid evolution of grid cell responses over the first moments of exploration, we propose that an underlying, preconfigured network process exists prior to departure from the nest. During the time representative of the first excursions from the nest, we explore how such a preconfigured, yet imprecise, network may autonomously refine.

In 2001, Song and Abbott emphasized the role of activity-independent processes and their importance in establishing underlying connectivity maps [40]. In their inspiration, we propose that the excitatory stellate cells found in MEC LII may be responsible for organizing the initial connectivity required for a continuous attractor network. Following the blueprint provided by the excitatory stellate cells, we investigate the recruitment of collocated inhibitory interneurons into the network. Using simple spike-timing dependent plasiticity (STPD) rules, we explore the development of the behavior of a network composed of disynaptically connected excitatory and inhbitory cells during

the early moments of exploration and experience. Our results represent a proof of concept that the combination of activity-independent and activity-dependent processes generate a stable continuous attractor network capable of producing grid cells.

II

Methods

Chapter 2

A Computational Model of Grid Cells

After their discovery in 2005, many efforts have been made to understand the contribution of grid cells within the entorhinal-hippocampal circuit as well as the mechanisms with which such distinct firing patterns could be generated. Addressing the latter topic, several distinct classes of computational models have been proposed that describe networks capable of generating cells with hexagonally-spaced firing fields. Within this thesis, we focus our investigation into the behavior of network models organized as continuous attractors. This chapter will contain a review of the dynamics of continuous attractor networks and the specific components that generate artificial grid cells.

2.1 A Continuous Attractor Network Approach to Modeling Grid Cells

Computational models founded upon continuous attractor dynamics generate neurons with grid cell-like responses by modeling a set of recurrently connected cells, representative of the excitatory stellate cells and inhibitory interneurons located in MEC layer II, and an excitatory drive into the recurrent network, often representing external input from the medial septum and hippocampus [5] [41] [42] [12]. This section will focus on the specifications of the model's recurrent and input populations and their biological analogues.

2.1.1 Continuous Attractor Dynamics

Generally, in a continuous attractor neural network, a recurrently connected set of neurons fall into a specific, stable state of activity given sufficient input. Often in the case of continuous attractor networks of grid cells, a set of neurons is arranged along a two-dimensional plane in which neighbors form inhibitory recurrent connections onto one another. As all connections are inhibitory, in the absence of external input, the recurrent network lies dormant, devoid of activity. However, when broad, excitatory input is provided to the recurrent population, the neurons within the network begin to fire. As neurons in the recurrent network become active, their inhibitory connections onto their neighbors suppress nearby activity, creating competition across the network. Given the proper balance

between recurrent inhibition and external excitation, the firing behavior in grid cell networks will manifest into stable activity packets in which the overall amount of possible activity is maximized. In the case of a recurrently connected population that lies along a planar space, these activity packets will form at the vertices of equilateral triangles, overall forming hexagonally patterned bumps of activity. This hexagonally tessellated activity space is described by Turing instability and is the stable state of the full population of the planar continuous attractor network [43].

While the above describes a network *population* activity that manifests into hexagonally patterned packets, we are interested in creating artificial grid cells with *individual* activity that exhibits spatially periodic patterns. In order to generate the desired activity within a single cell in the network, the stable, hexagonally patterned population activity can be shifted around the network in a smooth, continuous manner. When the shifting speed and directionality of the activity packets is appropriately coupled to the agent's velocity, the activity of individual grid cells within the network will inherently assume the stereotyped spatially periodic tessellation.

2.1.2 Recurrent Population

The recurrent population of the grid cell network model provides the required inhibition for the balanced continuous attractor dynamics. The components of this recurrent population are representative of the neurons and the connectivity observed within MEC LII. As reported by Couey and colleagues in 2013, MEC LII is predominantly populated with excitatory stellate cells that form abundant disynaptic connections with one another via fast-spiking, parvalbumin expressing inhibitory interneurons [5] [44]. These disynaptic connections allow for functional interdependence between the excitatory cells, although only via a mediating inhibitory neuron. In contrast to the plentiful connections observed between stellate cells and inhibitory interneurons, Dhillon and Jones reported that excitatory stellate cells almost never formed excitatory connections with one another [45]. The experimentally observed connectivity structure aligns with theoretical assumptions made within continuous attractor models of grid cell networks and is represented in the model's recurrent population, either explicitly or implicitly. In the implicit case, only excitatory stellate cells have a direct representation within the network. In a break with Dale's principle, the excitatory stellate cells form inhibitory synapses onto one another [46], thereby representing the disynaptic connection in a simplified manner. Alternatively, the disynaptic connection can be explicitly represented with the presence of both excitatory stellate cells and inhibitory interneurons that form appropriate synapses onto one another.

In both the cases of models with an explicit or implicit representation of inhibitory interneurons, stellate cells within the recurrent population are arranged evenly along a two dimensional surface. If the model explicitly includes inhibitory neurons, they will also be distributed evenly across the same plane. Excitatory stellate cells and inhibitory interneurons then form synapses onto their neighboring neurons, with the radius of connectivity and the weight profile given by model specifications. Given the proper model parameter tuning, an injection of feedforward excitation into the recurrent network should force either a single or multiple activity bumps to appear along the planar surface.

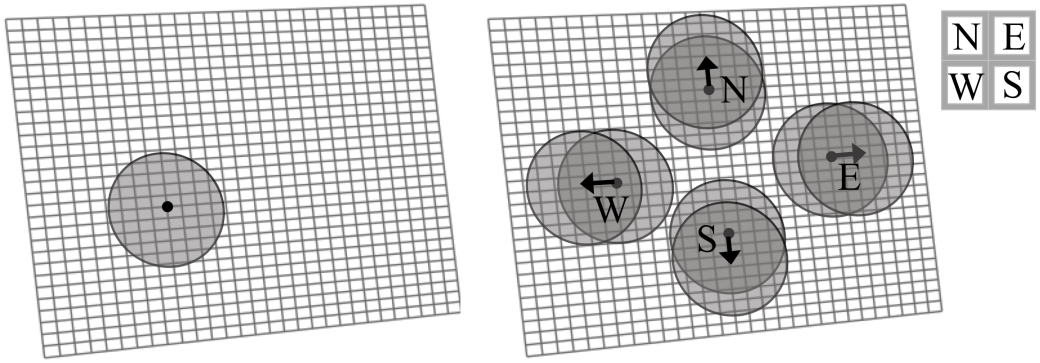

Fig. 2.1 An example of standard connectivity in which all neurons along the network plane form synapses to other neurons lying within a given radius. On the right, an example of the shifted connectivity required to translate activity across the attractor manifold. All neurons are given a *N,S,W,E* labeling, and their radius of connectivity is shifted in that direction. Neurons with a *N* direction preference are more sensitive to input representing a northbound trajectory. The small rightmost image indicates how the direction preferences are tiled across the network. Each 2x2 block of cells along the plane contains one of each of the direction preferences.

While a current injected into the recurrent network should begin to form hexagonally patterned bumps of activity, this simple planar representation of the putative grid cells is unstable as the network will suffer from edge distortions. Namely, cells located near the boundaries of the recurrent plane will receive fewer inhibitory inputs given their reduced number of neighboring cells. This will result in a non-uniform competition for activity within the network. One of two possible solutions can be implemented to avoid these defects: either the planar recurrent network can be wrapped into a torus configuration such as to force neurons near the edges to connect with one another, or the feedforward input into the network can be appropriately tapered with an envelope function such as to limit the activity at the boundaries. With the addition of either the twisted torus connectivity structure or the input tapering envelope function, a broad feedforward current projected into the recurrent network should now result in a stable, hexagonally patterned activity profile.

To produce the periodic spatial firing pattern within single cells of the recurrent network, the activity bumps must be translated along the continuous attractor manifold such that the speed of the translation of activity bumps aligns with the speed of the agent as it moves through space. One way to achieve this is to uniformly assign every cell within the recurrent population with a directional preference of motion and to shift the connectivity profiles between cells as per their directional preference [31]. In addition to a tonic feedforward input current to the network, an input current related to the velocity of the agent is injected such that cells with a directional preference aligned with the direction of actual motion will receive stronger excitation. Coupled with the shifted recurrent connections and the velocity-dependent input current, the hexagonally spaced activity peaks will translate across the recurrent network, generating individual cells that produce firing patterns with the spatial periodicity characteristic of grid cells.

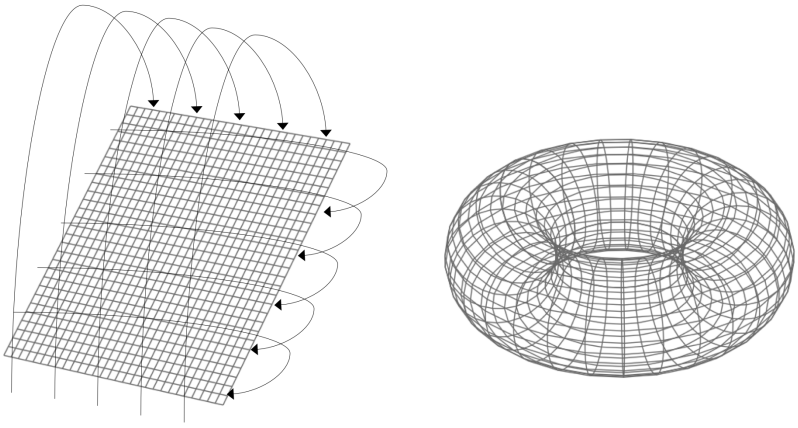

Fig. 2.2 Forming the recurrent population into a periodic torus. In order to avoid the edge defects of a planar continuous attractor network, the plane can be folded upon itself such that neurons lying along the edges are joined to form a torus, or donut shaped figure. Once assuming the toroidal shape, cells connect to one another in a radial fashion as in figure 2.1

2.1.3 Input Population

As described above, a strong feedforward tonic input as well as a velocity modulated input are critical for providing the excitation required to generate continuous attractor dynamics. Recent experimental findings indicate the presence and the importance of both the tonic excitatory input and the velocity modulated input into the recurrently connected network of cells in MEC LII. In 2013, Bonnevie and colleagues reported that inactivation of backprojections from the hippocampus to MEC resulted in the loss of spatial patterning in grid cell activity [12]. Additionally they reported that neurons that were originally classified as grid cells began to tune their firing activity towards the heading direction of motion after the lesion of hippocampal input. Taken together, the experimental findings indicate that a steady excitatory drive is required to maintain periodic grid cell activity as well as the possibility that heading direction input may also be supplied to the grid cell network that becomes predominant in the absence of the larger excitatory drive.

More recently, researchers have reported on the presence of speed modulated input extending from both within MEC LII and from regions that project to MEC LII. In 2015, a specific set of cells within MEC LII were identified as having a firing rate that linearly depended on the speed of the agent [22]. Later, in 2016 and 2017, researchers reported that the medial septum provides speed information into MEC LII [41] [42]. Taken together, the presence of a speed input and of a heading direction input jointly represent the velocity of an agent that would be required to translate the activity patterns across the continous attractor manifold.

Reflecting the experimental findings, the input population to the recurrent grid cell network consists of a broad excitatory current as well as a velocity-dependent current. As would be expected by its description, each cell in the recurrently connected population receives an equivalent excitatory

current. Given a sufficiently strong uniform injection, the current reflective of the hippocampal back-projections, will generate the hexagonally tessellated activity bumps within the recurrent population. If edge defects are managed via the envelope function described above, then cells in the recurrent population will receive an excitatory current dependent on their location on the recurrent plane and the parameters of the envelope function.

The velocity input is delivered to cells in the recurrent population in order to cause the patterned activity to appropriately translate across the continuous attractor manifold. As such, cells lying along the two dimensional recurrent population are each tagged with a directional preference of motion, and receive a conjunctive input of heading direction and speed in accordance with their preferred directionality. Cells in the recurrent population are more excited by motion corresponding to their preferred directionality. This differential excitation forces the patterned activity to translate across the attractor manifold such as to represent motion of the agent. As highlighted in the first chapter, this input could be represented by the heading direction and speed cells found in MEC LII and of the speed signal provided by the medial septum. When the velocity input to the recurrent population is appropriately tuned, it will force the activity bumps generated by the broad-field input to shift in sync with the motion of the agent, thereby causing the individual cells in the recurrent population to exhibit the firing properties of grid cells. To generate the velocity input used in all simulations, we create a random walk trajectory representative of an agent navigating in a circular arena over the course of three minutes.

In the following chapter, we present specific realizations of models that incorporate the recurrent population and an input current, representative of the input population, in order to generate grid cells through continuous attractor dynamics.

Chapter 3

Realizations of Continuous Attractor Grid Cell Network Models

We implement and design three realizations of grid cell networks with underlying continuous attractor dynamics. While the model specifications and parameter values are modified throughout the following implementations, each model generates artificial grid cells based upon the principles described in the previous chapter. All models are implemented in Python using the Brian2 neural network simulation package.

3.1 Rate-Based Model

In order to directly observe the dynamics of a continuous attractor model of grid cells, we begin by implementing the continuous attractor network model presented by Burak and Fiete [31]. As one of the first publications of a computational model capable of generating grid cell firing responses, the network structure minimizes complexity and stochasticity. The network composes a set of excitatory neurons arrranged onto a two dimensional field which form inhibitory synapses onto one another. A Gaussian kernel determines the synaptic weight between neurons such that neurons form increasingly strong inhibitory synapses with their more distant neighbors until a threshold radius where connectivity ends.

To couple the velocity of the agent to the motion of the activity bumps over the attractor manifold, the authors assign each neuron in the recurrent population with a direction preference: N, S, E, and W, as pictured in figure 2.1. These direction labels are spread evenly over the entire population such as to uniformly tile each 2x2 square of neurons with a N, S, E, and W preferring neuron. Neurons then form recurrent connections with their neighbors based on the Gaussian kernel whose center is shifted in the preferred direction of the presynaptic neuron. Neurons are assigned an x- and y- location along the recurrent plane corresponding to the total number of neurons in the network, $N = n\ x\ n$, with positions ranging from $(\frac{-n}{2}, \frac{-n}{2})$ to $(\frac{n}{2}, \frac{n}{2})$. These location assignments are used as input to the Gaussian kernel to determine the synaptic weight strength between neurons.

The rate-based neuronal dynamics are given by

$$\tau\frac{dv_i}{dt} + v_i = f[\sum_j W_{ij}s_j + B_i] \tag{3.1}$$

where v represents neuronal activation, W_{ij} represents the recurrent synaptic weights from neurons j onto neuron i, and B_i represents the feedforward input to neuron i. The function f is a nonlinear rectifier given by

$$f[x] = \begin{cases} x, & \text{if } x \geq 0 \\ 0, & \text{otherwise} \end{cases} \tag{3.2}$$

The synaptic weight matrix is given by

$$W_{ij} = W_o(\vec{x}_i - \vec{x}_j - l\vec{\delta}) \tag{3.3}$$

where $\vec{x}_i$ represents the x- and y- locations of postsynaptic neuron i, $\vec{x}_j$ represents the x- and y- locations of presynaptic neuron j, l represents the magnitude of the shift of the recurrent connections, and $\vec{\delta}$ represents a unit vector describing the neurons preferred directionality, namely $\vec{\delta}$ = [0,1] for neurons with a preference of North, $\vec{\delta}$ = [-1,0] for those preferring West, and so on.

The argument for the function of W_o is given by

$$W_o(\mathbf{x}) = ae^{-\gamma|\vec{x}|^2} - e^{-\beta|\vec{x}|^2} \tag{3.4}$$

where a, γ and β are scalar parameters that determine the width of the connectivity kernel.

The feedforward input, B_i to each neuron i is given by

$$B_i = A(\vec{x}_i)(1 + \alpha\vec{\delta} * \vec{v}) \tag{3.5}$$

Finally, in the case of an aperiodic network, the envelope function, A($\vec{x}_i$), for the feedforward input is given by

$$A(\vec{x}_i) = e^{-a_o(\frac{|\vec{x}|-R+\delta r}{\delta r})^2} \tag{3.6}$$

If the network assumes a periodic connectivity structure to form a twisted torus network, $A(\vec{x}_i) = 1$ for all neurons.

Values for parameters listed in the above equations are given in table 3.1.

At the beginning of the simulation, a uniform feedforward tonic input and a small independent input are provided to all neurons in the network. As the neurons begin to become active, clusters of activity form that suppress other nearby activity packets until the overall population activation is maximized, producing the hexagonally patterned peaks. Once pattern formation is complete, an

additional velocity input is provided to the network, with $\vec{v}$ assuming the following values each for 250ms (0, π/5, -π/2), totaling 750ms of input, to ensure the stability of the activity pattern. After the activity patterning has settled, velocity input corresponding to the motion of the agent is provided to the network. Artificial grid cells within the recurrent population then have a high neuronal activation level as the agent passes through the vertices of a hexagon along its trajectory.

While this rate-based implementation of a continuous attractor model of grid cells produces the spatially periodic responses observed in cells residing in MEC LII, the use of rate-based neurons eliminates the noise observed within biological systems, and limits its representational power. The authors do extend their model to include spiking dynamics for the neurons within the recurrent population by introducing neural firing governed by inhomogenous Poisson processes, however we proceed to develop a model composed of *Leaky Integrate-and-Fire* (LIF) neurons in order to better capture neuronal dynamics and to present a model that could be implemented on hardware applications.

Component	Parameter	
	Value	Unit
N	128*128	-
Simulation Timestep	.5	ms
τ	10	ms
l	2	-
γ	1.03* β	-
β	3/λ	-
λ	13	-
a	1	-
α	0.10315	-
a_o	4	-
R	64	-
δr	64	-

Table 3.1 Rate-Based Model Parameters

3.2 Single Population Spiking Model

We design and implement a computational model of grid cells exhibiting LIF spiking dynamics. From the expansion of the model described above to include stochasticity in the spiking neurons, additional interpretations of the actual dynamics underlying a biological grid cell network may be made, such as the stability of the network behavior over extended simulations.

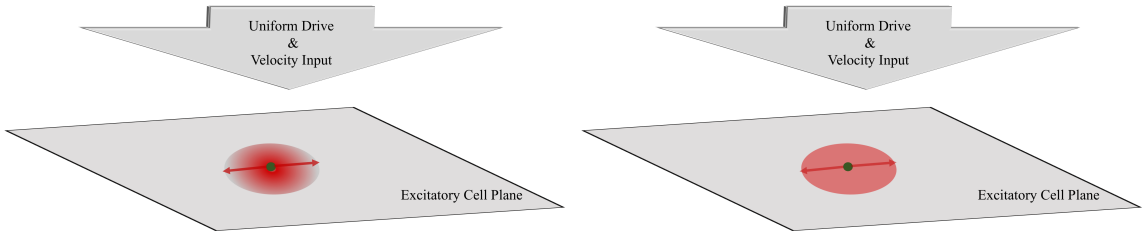

Fig. 3.1 Network construction of the rate-based and single population spiking model. In both models, excitatory cells form inhibitory connections with neighboring cells along the continuous attractor plane. The radius of connectivity is given by the network parameters. In the rate-based model, connections are given precise weights based upon a Gaussian kernel. The single population spiking model has been simplified to incorporate a uniform connectivity kernel such that all connections have the same synaptic weight. In both models, excitatory cells are assigned a directional preference that shifts their connectivity kernel as described in figure 2.1.The planar population can be either aperiodic or twisted into a torus configuration as shown in figure 2.2.

As in [31], cells within the recurrent population of the spiking network are arranged along a two dimensional sheet and assigned a location, $\vec{x}$, in the range$(\frac{-n_{row}}{2}, \frac{-n_{col}}{2})$ to $(\frac{n_{row}}{2}, \frac{n_{col}}{2})$ as well as a directional preference from the set N, S, E, and W.

The neuronal activation of neurons within the recurrent population is described by *LIF* spiking dynamics.

$$\tau \frac{dv_i}{dt} = v_r - v_i + R_m f(\vec{x}_i)(I_{vel} + I_{ext}) \tag{3.7}$$

where I_{ext} is the constant feedforward current that is set constant throughout the simulation, and the velocity-dependent current, I_{vel}, is given by

$$I_{vel_i} = vel_{drive} * (\vec{x}_i \cdot \vec{m}) \tag{3.8}$$

where $\vec{m}$ is the speed of the agent in m/s and vel_{drive} is a scalar value set to appropriately couple the translation of network activity with the motion of the agent.

When the network is configured to be periodic, neurons lying along the edges connect with one another. If the network is configured to be aperiodic, the value of the envelope function, $f(\vec{x}_i)$ is calculated by

$$f(\vec{x}_i) = e^{-a\frac{\sqrt{{x_i}^2+{y_i}^2}}{n_{col}}} \tag{3.9}$$

where n_{col} represents the magnitude to which the recurrent population extends along the *y-axis*.

We further simplify the rate-based model by introducing a simpler connectivity scheme, without the need for a precise Gaussian kernel. Instead, neurons connect given by

$$W_{ij} = \begin{cases} w, & \text{if } |\vec{x}_i - \vec{x}_j - l\vec{\delta}| \leq R \\ 0, & \text{otherwise} \end{cases} \tag{3.10}$$

Here again, cells connect recurrently in a shifted manner dependent on their directional preference, δ, and the scalar shift parameter l.

Values of all parameters listed in the above equations are given in table 3.2.

At the onset of the simulation, artificial grid cells are initialized with a random membrane potential and the uniform feedforward current and motion related input is immediately provided. Similar to the rate-based model presented in the previous section, activity bumps quickly emerge and rapidly transition into the hexagonally tiled pattern which is shifted over the continuous attractor manifold. Importantly, results from the spiking model confirm that broad feedforward input and velocity input may be provided to the network simultaneously, and that this input quickly results in patterned population activity. In contrast to the rate-based model, the spiking model does not require a biologically implausible pattern initialization period. We further extend this spiking model to include an explicit representation of the fast-spiking inhibitory interneurons found within MEC LII.

Component	Parameter	
	Value	Unit
Excitatory Cell Rows	132	-
Excitatory Cell Columns	112	-
Simulation Timestep	1	ms
Excitatory Cell Resting Potential	-65	mV
Excitatory Cell Reset Potential	-67	mV
Excitatory Cell Threshold Potential	-63	mV
Excitatory Cell Membrane Time Constant	10	ms
Excitatory Cell Membrane Resistance	10	Ω
Excitatory Cell Refractory Period	5	ms
External Input Current	2.4	mA
Velocity Current	0.175	mA
Orientation Preference Shift	2	-
Synaptic Weight	-0.6	mV
Synaptic Delay	5 * rand()[1]	ms

Table 3.2 Single Population Spiking Model Parameters

[1]The function rand() adds a random number between 0-1 to each of the synapses, resulting in synaptic delays between 5-6ms

3.3 Dual Population Spiking Model

While the spiking model presented in the previous section produces neurons with grid cell responses, it contains a reduced representation of the actual connectivity found in MEC LII. In this section we describe a model designed and implemented to include an explicit population of spiking inhibitory neurons.

The network consists of $N_E = n_{row_e}\ x\ n_{col_e}$ excitatory stellate cells and $N_I = n_{row_i}\ x\ n_{col_i}$ inhibitory interneurons with a recurrent connectivity scheme. Once more, excitatory stellate cells are arranged along a two dimensional sheet and assigned a location, $\vec{x}$, in the range($\frac{-n_{row_e}}{2}$,$\frac{-n_{col_e}}{2}$) to ($\frac{n_{row_e}}{2}$,$\frac{n_{col_e}}{2}$) as well as a directional preference from the set *N*, *S*, *E*, and *W*. The inhibitory interneurons are aligned along this same plane. The inhibitory population, which consists of fewer neurons than the excitatory stellate cell population, are stetched to extend evenly over the full width and length of the larger population with locations between ($\frac{-n_{row_e}}{2}$,$\frac{-n_{col_e}}{2}$) to ($\frac{n_{row_e}}{2}$,$\frac{n_{col_e}}{2}$). Inhibitory neurons are not assigned a directional preference.

The neuronal dynamics of the spiking stellate cells are given by equation 3.6, with I_{vel} given by equation 3.7. The dual population is configured in an aperiodic manner where the value of I_{ext} is controlled by the envelope function, $f(\vec{x}_i)$, by

$$f(\vec{x}_i) = e^{-a\frac{\sqrt{{x_i}^2+{y_i}^2}}{n_{col_e}}} \tag{3.11}$$

Inhibitory interneurons receive input only from the excitatory stellate cells within the recurrent population. They are not excited by either I_{ext} or I_{vel}.

The neuronal dynamics of the inhibitory neurons are given by

$$\tau\frac{dvi_i}{dt} = vi_r - v \tag{3.12}$$

Unlike the connectivity structure of the single population spiking model, excitatory stellate cells do not form any synapses onto other stellate cells. Rather, in accordance with Dale's principle, they make excitatory connections with the inhibitory neurons within the network. The connectivity rule between stellate cells, *i*, onto inhibitory cells, *j*, is given by

$$W_{ij} = \begin{cases} w_{EI}, & \text{if } |\vec{x}_i - \vec{x}_j - l\vec{\delta}| \leq R_{EI} \\ 0, & \text{otherwise} \end{cases} \tag{3.13}$$

Similarly, the inhibitory cell population form synapses onto only cells in the excitatory stellate cell population given by

$$W_{ij} = \begin{cases} w_{IE}, & \text{if } |\vec{x}_i - \vec{x}_j| \leq R_{IE} \\ 0, & \text{otherwise} \end{cases} \tag{3.14}$$

Values of all parameters listed in the above equations are given in table 3.3. Membrane potential parameters, EPSP and IPSP values, and connectivity rates were derived from [47] and [5].

As with the single population spiking model, the membane potentials of stellate cells and inhibitory interneurons are randomly initialized. Stellate cells receive a uniform feedforward current that is scaled by equation 3.10 and velocity current immediately upon simulation start. Similar to the single population model presented in the previous section, activity bumps quickly emerge and rapidly transition into the hexagonally tiled pattern which is shifted over the continuous attractor manifold.

With the development of this dual population spiking model, we are able to extend our investigation into biologically plausible dynamics of a continuous attractor network model of grid cells. In the next chapter, we describe the implementation of spike-timing dependent learning rules implemented within the system that can be used to elucidate ways in which an imprecise network, endowed with an underlying connectivity structure, may refine with time and experience.

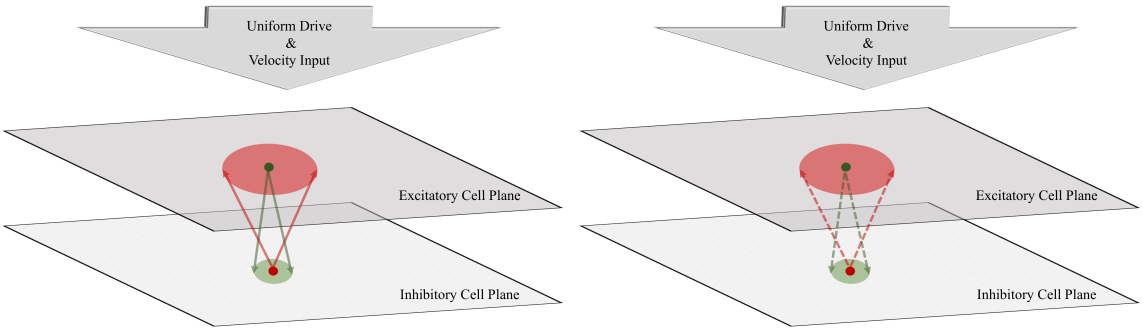

Fig. 3.2 Network construction of the dual population spiking model and the dual population spiking model incorporating STDP. Both models introduce an inhibitory population of cells. The excitatory stellate cells and inhibitory cells are uniformly distributed along the same two dimensional plane, shown here as two separate planes strictly for visualization. Excitatory stellate cells form excitatory connections with inhibitory cells and inhibitory cells form inhibitory connections with stellate cells, both within designated radii. The feedforward input is provided only to the excitatory population which in turn activates the inhibitory cells. Each cell in the excitatory population is assigned a directional preference that shifts its connectivity kernel as described in figure 2.1. The planar population in both models is configured to be aperiodic, with feedfoward input scaled by an envelope function. As as described in chapter 4, the dual population spiking model with STDP explores the affect of plasticity on both the excitatory and inhibitory synapses, designated by the dashed connections.

Component	Parameter	
	Value	Unit
Excitatory Cell Rows	132	-
Excitatory Cell Columns	112	-
Inhibitory Cell Rows	66	-
Inhibitory Cell Columns	58	-
Simulation Timestep	.5	ms
Excitatory Cell Resting Potential	-60	mV
Excitatory Cell Reset Potential	-65	mV
Excitatory Cell Threshold Potential	-55	mV
Excitatory Cell Membrane Time Constant	10	ms
Excitatory Cell Refractory Period	5	ms
Excitatory Cell Membrane Resistance	10	Ω
Excitatory Cell Refractory Period	5	ms
Inhibitory Cell Resting Potential	-68	mV
Inhibitory Cell Reset Potential	-70	mV
Inhibitory Cell Threshold Potential	-62	mV
Inhibitory Cell Membrane Time Constant	3	ms
Inhibitory Cell Refractory Period	2	ms
External Input Current	2.1	mA
Velocity Current	0.24	mA
Orientation Preference Shift	2	-
Excitatory Synaptic Weight	1.8	mV
Inhibitory Synaptic Weight	-1.1	mV
Excitatory Synaptic Delay	.5 + rand()	ms
Inhibitory Synaptic Delay	.5 + rand()	ms

Table 3.3 Plasticity-Enabled Dual Population Spiking Model Parameters

Chapter 4

Autonomously Refining Continuous Attractor Model of Grid Cells

While the grid cell network models presented in the previous chapter all produce neurons that fire in a spatially periodic pattern, they all compose of strictly hardwired connections. Spike-timing dependent plasticity couples the synaptic strength between two neurons to the correlation of their spiking activities, and is a learning phenomena that has been reported within MEC LII [47]. Having developed a functioning dual population model of grid cells reminiscent of the actual connectivity within MEC LII, we now wish to investigate the effects of STDP rules on the behavior of the network. We primarily see to explore two questions:

1. *Given an imprecise network configuration equipped with STDP rules, does the network refine through experience towards more precise continuous attractor dynamics that produce cells with grid cell responses?*

2. *Given the introduction of STDP rules into the recurrently connected network, do the continuous attractor dynamics remain stable and continue to produce individual cells with grid cell responses?*

These questions address the plausability of a network generated by both activity-independent and activity-dependent processes. If network simulations result in stable continuous attractor dynamics that rapidly produce grid cells, then a coordinated connectivity strategy introduced by excitatory stellate cells could be sufficient to describe the development of the grid cell network in MEC LII.

4.1 Spike-Timing Dependent Plasticity in MEC LII

Traditional *Hebbian* STDP induces changes in synaptic weights based upon the timing of pre- and postsynaptic spikes. Most commonly, reports of STDP involve excitatory presynaptic cells, and in the instance of several publications, excitatory presynaptic cells specifically onto inhibitory postsynpatic

cells [48] [49] [50] [51]. While many fewer publications report of STDP from inhibitory presynaptic cells onto excitatory postsynaptic cells, one of the seminal reports of this phenomena described the behavior of plasticity between these two cells classes within MEC LII [47]. This *anti-Hebbian* STDP behavior has asymmetrical dynamics similar to that of traditional Hebbian STDP, in which the strength of a synapse is strengthened or weakened depending on the timing of pre- and postsynaptic spikes.

Anti-Hebbian STDP dynamics of inhibitory synapses reflective of those reported by Haas and colleagues was implemented into the dual population model. While are not yet specific reports of STDP behavior of excitatory cells in MEC LII, we implement a learning rule commensurate with the dynamics describing learning between excitatory presynaptic cells and inhibitory postsynaptic cells.

4.2 Modeling Spike-Timing Dependent Plasticity in the Dual Population Spiking Network

In the dual population spiking model, connections from both the excitatory onto inhibitory and from the inhibitory onto excitatory populations are equipped with spike time-dependent learning rules. The windows for STDP from excitatory onto inhibitory neurons are given by the following kernels,

$$\Delta W_{ij} = \begin{cases} k_+ = Ae^{-t/taupre_{EI}}, & \text{if } t_{pre} \leq t_{post} \\ k_- = -ae^{-t/taupost_{EI}}, & \text{if } t_{post} \leq t_{pre} \end{cases} \tag{4.1}$$

The windows for STDP from inhibitory onto excitatory neurons are given by,

$$\Delta W_{ij} = \begin{cases} k_+ = Be^{-t/taupre_{IE}}, & \text{if } t_{pre} \leq t_{post} \\ k_- = -be^{-t/taupost_{IE}}, & \text{if } t_{post} \leq t_{pre} \end{cases} \tag{4.2}$$

Both the traditional Hebbian STDP and the anit-Hebbian STDP learning kernels are visualized in figure 4.1. Parameter values for the STDP equations are given in table 4.1.

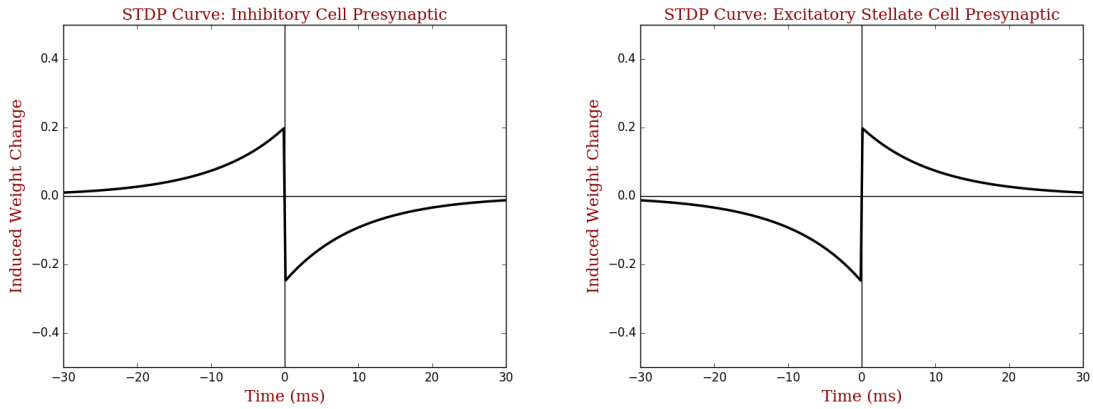

Fig. 4.1 Inhibitory and Excitatory STDP Kernels

Component	Parameter	
	Value	Unit
$taupre_{EI}$	10	ms
$taupost_{EI}$	10	ms
$wmax_{EI}$	2.8	mV
A	.2	-
a	.25	-
$taupre_{IE}$	10	ms
$taupost_{IE}$	10	ms
$wmin_{IE}$	-2	mV
B	.25	-
b	.2	-

Table 4.1 STDP Model Parameters

III

Results

Chapter 5

Model Simulation Results

We report on both the population and single cell behavior of the continuous attractor network models of grid cells described in the previous chapters. Generally we find that models of increasing complexity provide an increasing understanding of the network mechanisms required for the generation of individual grid cells. We find that increased stochasticity in the network demands an additional anchoring force to reliably reproduce grid cells. Reported gridness score are computed as in Sargolini et al and their computation is described in detail in appendix 2 [52].

5.1 Results of Rate-Based Model Simulations

While the rate-based model is capable of producing grid cells, it has a number of biological and technological disadvantages. From the technological perspective, the rate-based connectivity scheme requires that the activation level of each neuron be updated to include the synaptic input from each of its presynaptic neurons at each time step, rather than on each spiking event. This dramatically increases the overall simulation time. Our implementation in Python required more than ten minutes of actual time to complete one second of simulation time. Lengthy simulation times were prohibitive of evaluating network activity over an extended trajectory.

Biologically speaking, the results of the rate-based model are difficult to evaluate for plausibility in that the network requires a specific initialization period of non-trivial length before it is capable of tracking agent motion. Specifically, the network required more than two seconds of simulation time for a stable, spatially tessalated population activty pattern to form, and only thereafter was capable of receiving velocity input. Without this exclusive initialization period, the network was unable to produce the expected hexagonally patterned activity bumps.

Figures 5.1 and 5.2 display the population activity of the two-dimensional, aperiodic network during the initialization period. In figure 5., the leftmost image depicts network activity immediately after injection of the feedforward current. Resultant from the envelope function, the largest activity clusters at the center of the network, and is represented in red. The middle image represents network activity after 50ms of injected current, where distinct bumps of activity begin to form. Finally, the

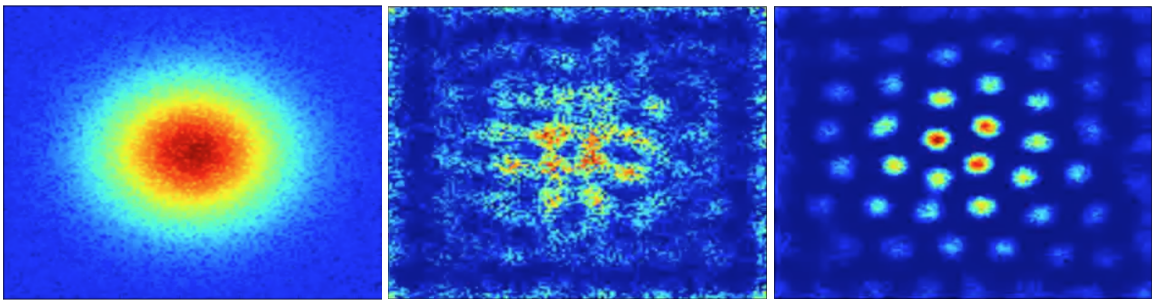

Fig. 5.1 Early pattern formation in the rate-based network. The network activity represents the individual activation of cells in the recurrent population distributed over a two dimensional surface. Population activity is shown immediately after injection of feedforward current, and then again after 50ms and 250ms.

rightmost image depicts activity after 250ms. At this point, the activity bumps become more defined and begin to shift towards a hexagonal pattern.

After continued feedforward input the population activity refines, as is shown in figure 5.2. While the patterning is relatively stable after 750ms of injected current (figure 5.2, left), the precision of the angles between activity bumps refine towards forming a more perfect hexagon after 1750ms (figure 5.2, right). The initialized network is then capable of tracking motion with the input of velocity current.

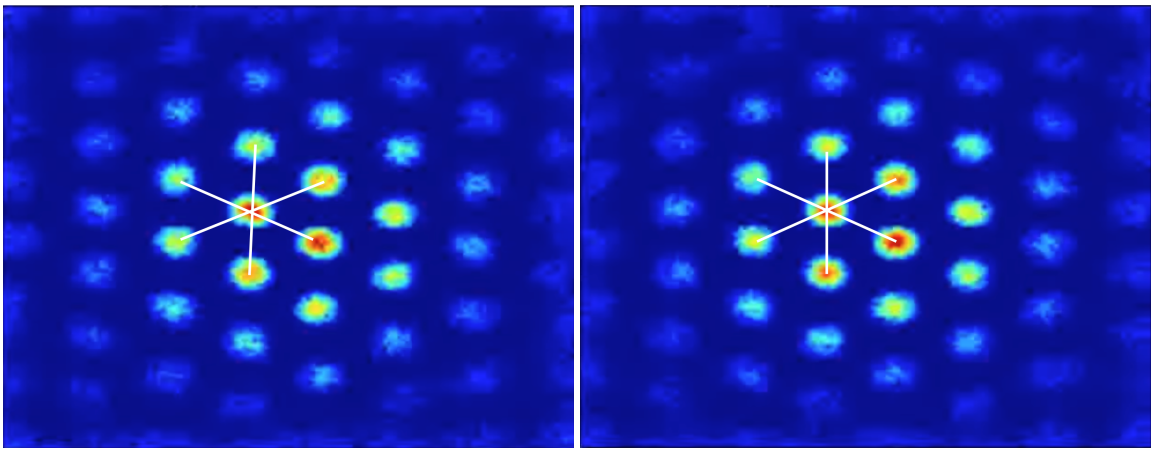

Fig. 5.2 Final pattern refinement in the rate-based network. The left image depicts population activity at 750ms and right at 1750ms. After the initial patter formation, network activity slowly stabilizes into precise continuous attractor bumps, forming a distinct hexagonal pattern.

5.2 Results of Single Population Model Simulations

Using the simple, uniform connectivity pattern in the recurrent population, the spiking The computation of the grid score of each cell in the network is expensive so we instead randomly select neurons from the recurrent network for evaluation.

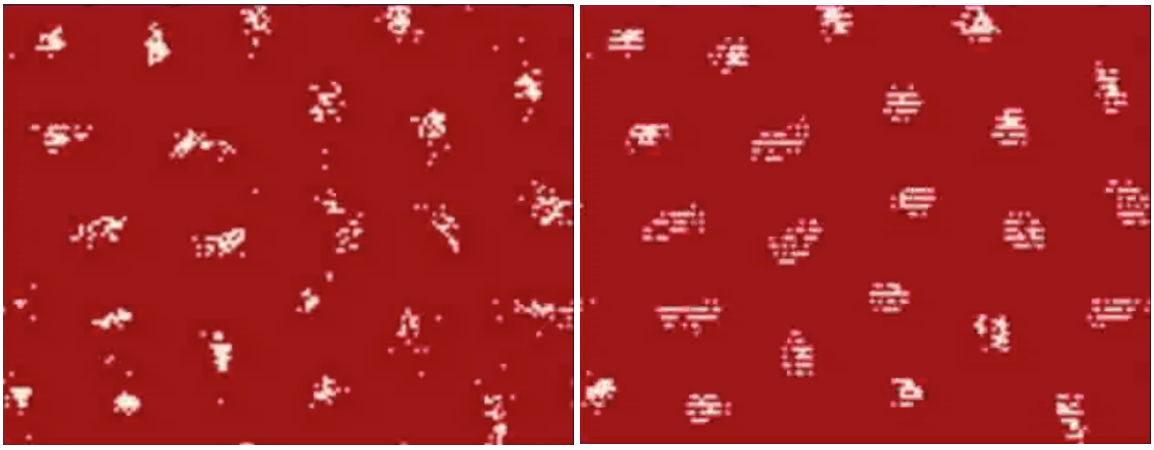

Fig. 5.3 Pattern formation in the single population spiking network. From left to right, the images depict population activity at 100ms and at 250ms.

Figure 5.3 depicts early pattern formation in the single population spiking network. The left image shows activity after 100ms and the right shows early population stability at 250ms. In contrast to the rate-based network, the spiking model is able to develop a stable, hexagonally patterned population activity while simultaneously integrating velocity inputs.

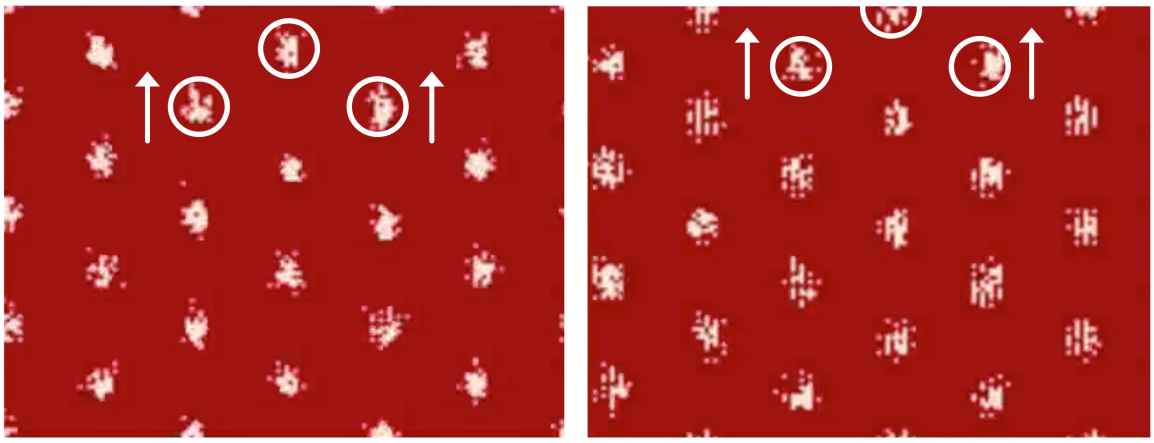

Fig. 5.4 Translation of population activity across the attractor manifold over several seconds of motion. As the agent moves *upward*, velocity inputs reflecting the motion cause the population activity to shift in the respective direction. Here the motion is primarily upward and very slightly to the right.

Figure 5.4 displays the translation of population activity across the attractor manifold over the course of several seconds of motion. Given the correct coupling between velocity inputs and agent motion, the translation of population activity results in individual cells that spike at the vertices of equilateral triangles. Figure 5.5 displays such activity. We simulated the behavior of the recurrent grid cell network over the course of a three minute trajectory meant to characterize the motion of an agent within a circular arena. At the conclusion of the simulation, the spiking activity of one of the neurons in the recurrent population was overlaid onto the trajectory such that the red dots represented the location of the agent at each spike time. As can be seen, the spikes cluster into a hexagonal pattern and meet the criteria for grid cells. The center figure in 5.5 represents the average firing late in each location within the arena, which is used to create the spatial autocorrelogram on the right. The depicted cell has a grid score of 0.554, indicating a strong periodic spatial representation comparable with the scores of grid cells reported in Hafting et al [2]. Repeated simulations showed similar results for other randomly sampled cells in the network.

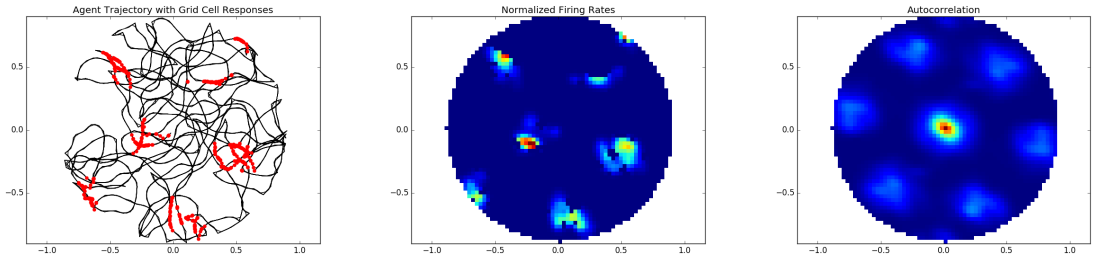

Fig. 5.5 Results of an individual grid cell from the single population spiking model. The leftmost image depicts the grid cell activity overlaid onto the agent's trajectory. The center image reflects the normalized firing rate over the arena space. On the right, the autocorrelogram of the normalized firing rate is used to calculate the gridness score of 0.554

Unlike the deterministic rate-based model, the use of neurons with leaky integrate and fire spiking dynamics with synaptic delays and refractory periods, introduces drift into the population activity of the network. This ultimately results in the translation of the population activity becoming decoupled from the actual motion of the agent. Over time, this will force the spiking activity of the individual cells to deviate from the more precisely patterned hexagonal activity. While the accumulated error is limited in the three minute trajectory depicted in figure 5.5, the pattern significantly reduces over longer simulations. Experimental reports of in-vivo grid cell recording often extend over ten to twelve minute trajectories, however, the error accumulated in the computational model requires some additional grounding element to maintain proper motion tracking.

Possible mechanisms for the temporal stability of continuous attractor network models of grid cells have been identified as both border cells and sensory cues reminiscent of place cells [53] [54]. As described in the first chapter, both border cells and place cells are spatial representation cells found along the entorhinal-hippocampal circuit. Hardcastle et al showed that environmental boundaries

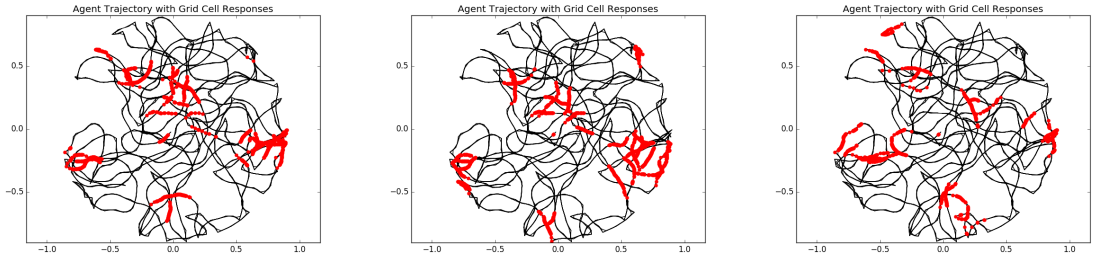

Fig. 5.6 Additional sampled grid cells from the single population spiking model.

were critical for the maintenance of grid cells both in behaving rodents and in extended simulations of continuous attractor based computational models. Similarly, Mulas and colleagues generated an extended model that included a continuous attractor network representing grid cells and a sensory network representative of place cells. The addition of input from the sensory network generated longer stability in the simulations of artificial grid cell networks.

5.3 Results of Dual Population Model Simulations

Explicitly representing the inhibitory and excitatory cells found in MEC LII, the dual population model better represents the biological connectivity of a grid cell network. Similar to the single population spiking model, the dual population model requires no initialization period. Once properly configured, both the broad, feedforward input current and the velocity input are delivered to the excitatory cells in the model which in turn activate the inhibitory interneurons. Within several hundred milliseconds of input, the hexagonally shaped population pattern stabilizes and begins to shift along the attractor manifold in accordance with velocity input. As depicted in figure 5.8, the excitatory cells in the dual population network also produce grid cell responses.

Similar to the single population spiking model, this more complex implementation is subject to the effects of drift accumulated over simulation time. As the spiking dynamics of cells both in the excitatory and inhibitory populations contribute imprecision to overall network activity, the population pattern can more quickly decouple from the motion of the agent, which in turn limits the stability of individual grid cells. Here again, as described in Hardcastle et al and Musal et al, the introduction of a population of cells representing place cell or border cell input could reduce drift and imprecision in the model.

5.4 Results of Plasticity-Enabled Dual Population Model Simulations

In addition to investigating the underlying connectivity in MEC LII, Couey and colleagues also reported on the expression of parvalbumin in the putative grid cell network in postnatal development. They reported that the amplitudes of inhibitory synapses (IPSPs) increased dramatically form P15, just

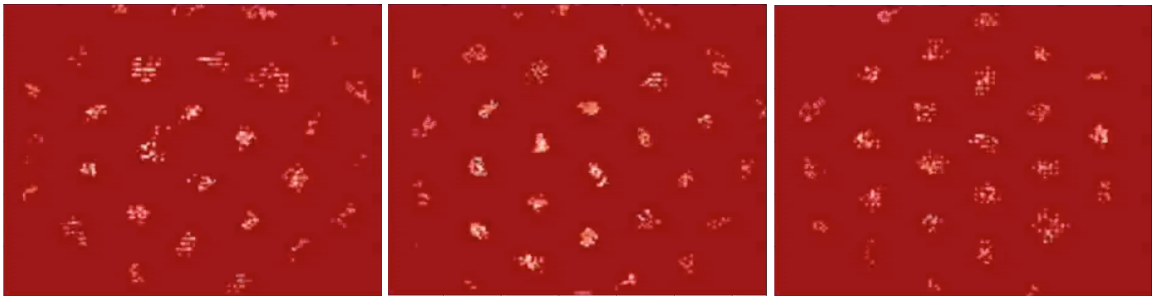

Fig. 5.7 Population activity in the dual population model quickly begins to exhibit hexagonal patterning that stabilizes within the first seconds. Images from left to right represent activity at 300ms, 800ms, and 2500ms after onset of feedforward input into the recurrent population of excitatory stellate cells. As the network has aperiodic boundaries, an envelope function tapers feedforward input near the network edges which causes activity to be centered in the middle of the recurrent population.

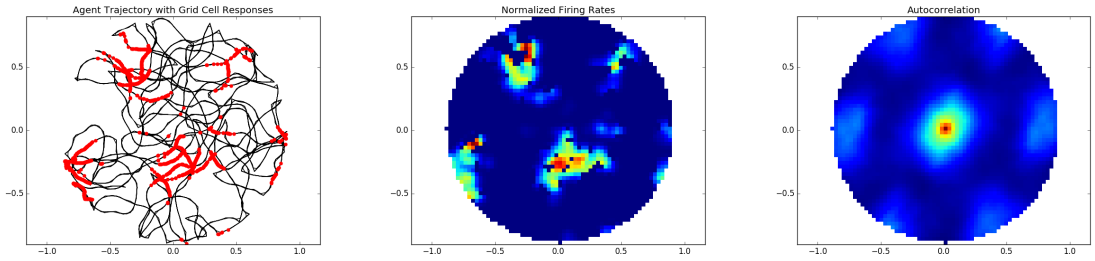

Fig. 5.8 Results of an individual grid cell in the dual population spiking model, reflecting a gridness score of 0.463

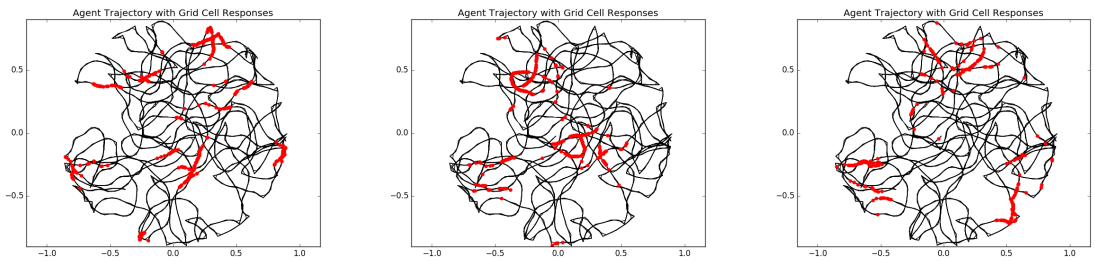

Fig. 5.9 Additional sampled grid cells from the dual population spiking model.

prior to the first exploration from the nest, to P28 [5]. As indicated in Donato's 2017 findings on the structural maturation of cells along the entorhinal-hippocampal circuit, the parvalbumin expressing inhibitory cells located in MEC LII increased their synaptic density only after stellate cells in the same region exhibited high levels of maturation [26]. Taken together, the functional maturation of the grid cell network could be facilitated by an increase in inhibitory synaptic strength guided by the activity of mature excitatory stellate cells. We therefore explore the behavior of our spiking dual population grid cell model when synaptic plasticity allows for a marked increase in inhibitory synaptic strength.

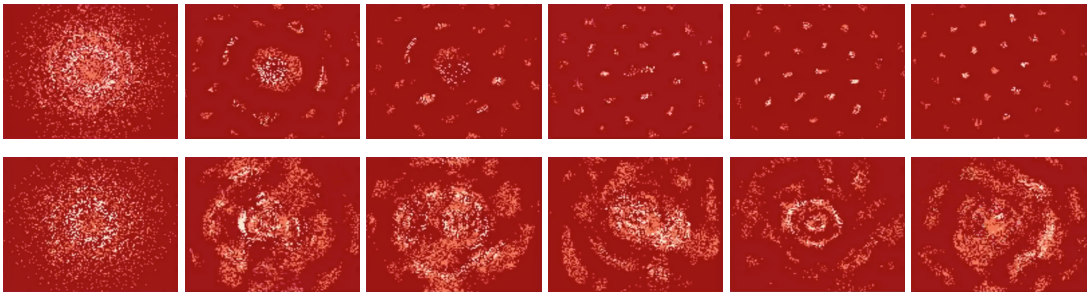

Fig. 5.10 The top row of figures depicts the progression of the population activity of a dual population, plasticity-enabled grid cell network over the course of a six second simulation. Below, is the progression of population activity in a dual population grid cell network without plasticity. In both aperiodic networks, the feedforward input current is injected while velocity input current is set to zero. Aligning with experimental findings, the strength of inhibition in the network is initially set very low with all inhibitory synapses set randomly between *0 to -.3 mV*. Activity of the excitatory cells, generated by the input current, drives activation of the inhibitory cells which in the case of the plasticity-enabled network, allows inhibitory synapses to strengthen. The set of images depicts the refinement of activity in the plasticity-enabled network. All other parameters in both networks are set as in table 3.3. Images in both rows represent, from left to right, activity immediately after injection of input current, at 100ms, 250ms, 500ms, 1000ms, and finally 6000ms. As is pictured, the plasticity-enabled network is capable of quickly refining population activity such as to generate stable continuous attractor dynamics. Without the introduction of STDP rules, the population activity of the network depicted in the lower row remains unstable.

Simulations depicting the refinement of population activity when plasticity is enabled for both inhibitory and excitatory synapses indicates that simple STDP rules could advance continuous attractor dynamics in a network seeded by coordinated excitatory stellate cell activity. With this first confirmation, we then explore the behavior of network population when inhibitory cells form probabalistic connections to nearby excitatory stellate cells. As before, network parameters are set as in table 3.3, with three exceptions: velocity input is set to zero, the strength of inhibitory synapses are set randomly between 0 and -0.3mV, and inhibitory cells form synpases within the specified radius of connectivity with the probability of each connection being made set to 70% . As with the previous network formulation, we again find that simple plasticity rules are sufficient to refine network activity even in this more imprecise network. Results are depicted in figure 5.11.

Given the reliable refinement of population activity, we now explore the behavior of individual grid cells in a plasticity-enabled dual population network. As before, both excitatory and inhibitory

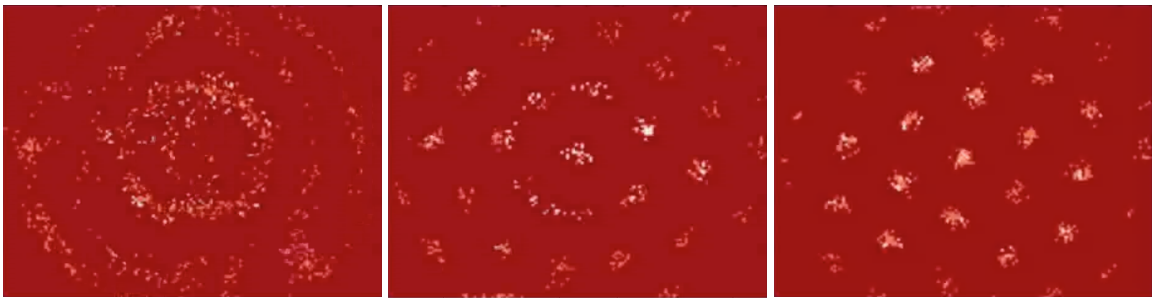

Fig. 5.11 Population activity refinement of the plasticity-enabled dual population spiking model with probabilistic connections. Population activity is shown at 100ms, 300ms, and with a stable, precise patterning at 6000ms. Even with initially low inhibition and probabilistic connections formed between inhibitory interneurons and excitatory stellate cells, simple STDP rules enable pattern refinement.

synapses are fit with the STDP rules described in chapter 4. We then simulate a network provided with parameters listed in table 3.3 to evaluate the stability of individual grid cells given that both velocity inputs are provided and plasticity is possible.

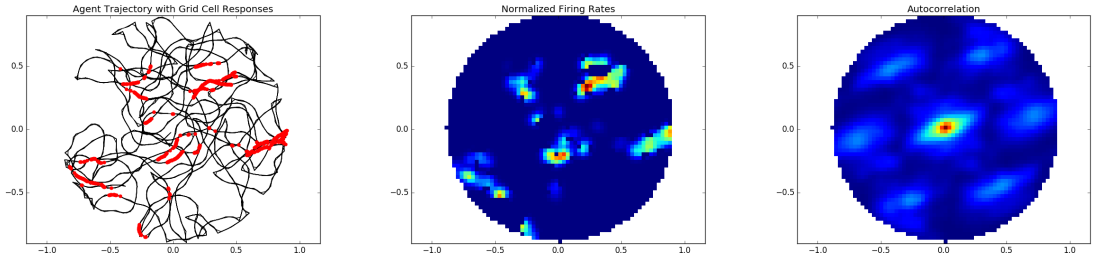

Fig. 5.12 Individual results of a grid cell sampled from the plasticity-enabled dual population spiking network. The behavior of the sampled grid cell indicates that STDP rules enabled even during motion allow for stable performance, here resulting in a grid score of 0.339

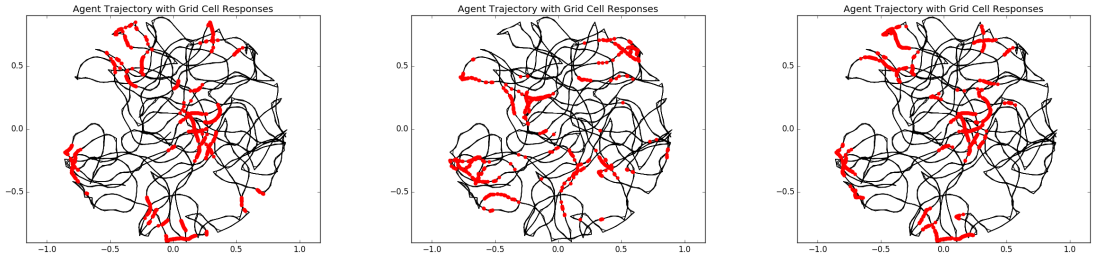

Fig. 5.13 Additional sampled grid cells from the plasticity-enabled dual population spiking model.

As indicated in figure 5.12, individual grid cells in the plasticity-enabled dual population network are stable. As before, the explicit modeling of both an excitatory and an inhibitory population introduces more drift into the continuous attractor network that ultimately reduces its temporal stability from the rate-based and single population spiking networks.

IV

Discussion

Chapter 6

Discussion of Model Results and Implications

In this thesis we have presented a selection of increasingly biologically plausible grid cell network models founded upon continuous attractor dynamics. We introduced a novel construction of a dual population spiking model consistent with the experimental findings of connectivity between principal excitatory cells and inhibitory interneurons, and their disynaptic connections, found in MEC LII. Seeking to elucidate the role of synaptic plasticity during the early postnatal development of neuronal circuits in MEC LII, we introduced simple STDP rules into the dual population model. The introduction of plasticity into our model demonstrated that basic STDP rules are capable of refining the population behavior of a dual population network and of producing individual cells with the spatially periodic response characteristic of grid cells.

6.1 Time Scale of Refinement

In the plasticity-enabled dual population spiking network, we showed that a seeded connectivity map provided by the excitatory stellate cells was sufficient to produce a stable network of grid cells. The provided results indicate that the refinement of the network occurs very abruptly over the course of several seconds once excitatory feedforward input is provided. Results from the experimental studies of the functional development of grid cells indicate that this refinement could occur over a more protracted period during early postnatal exploration. These dissimilar time courses are not necessarily contradictory of our proposed model. In model simulations, all excitatory stellate cells immediately receive a uniform, strong feedforward input current. Biologically, this current may take additional time to appear and strengthen, which would elongate the period of time required to refine the network connectivity. Additionally, at the onset of model simulations, all structural connections are already established. The simulation time is then used to strengthen or weaken these synapses until the network stabilizes. During early postnatal life, just prior to departure from the nest, all of

the structural connections may not yet be present. If these connections were made over an extended period, the network refinement time would also be lengthened.

6.2 Plausibility of a Stellate Cell Seeded Network

The dual population, plasitcity-enabled spiking network relies on excitatory cells that display a coordinated connectivity strategy to create an initial, underlying network map. In contrast, the connections formed from inhibitory cells onto excitatory cells follow a simple connectivity rule. Namely, inhibitory cells should form structural connections with neighbors up to a given radius. As demonstrated in figure 5.11, these synapses may also be made imprecisely within the connectivity radius. When feedforward input is provided to the excitatory cells in the recurrent network, simple STDP rules drive the inhibitory synapses to strengthen until the whole network exhibits stable continuous attractor dynamics.

In Song and Abbott's 2001 publication, the authors emphasized the importance of activity-independent processes in the generation of underlying connectivity maps that form the basis of the overall network structure. In the dual population model, would it be possible that the excitatory stellate cells generate this initial network map? Supporting this possibility, several publications have reported on the coordinated activity of clonally related excitatory cortical cells. In 2012, Li et al reported that clonally related cells in the visual cortex had similar feature selectivity [55]. Clonally related cells in cortex exhibiting coordinated activity introduces the possibility that clonally related cells in MEC, a transition region between the allocortex and the neocortex, may also be instrumental in generating united network activity. As reported in Donato et al, the excitatory stellate cells in MEC LII, unlike all other cell types found in the region, are spatially distributed in accordance with their birthdate. This unique distribution lends credence to the notion that clonally related cells may coordinate to produce cells with similar orientation specificity in a grid cell network in MEC LII.

Prior to Li's 2012 publication, Yu and colleagues reported that excitatory sister cells were prone to form excitatory connections with one another [56]. Although connections between excitatory cells in the adult MEC LII are not present, Couey's 2013 publication reported the presence of early postnatal connections between excitatory cells that diminished in number between postnatal days P15-P27 [5]. In an earlier study of the electroresponsiveness of cells in MEC LII, Alonso and colleagues reported that stellate cells were activated after minimal changes of 1-3mV in membrane potential [57]. If stellate cells are highly responsive to input, then could minimal connections between sister cells in MEC LII be sufficient to generate activity? If so, could they form the basis of a two-dimensional synfire chain that recruits nearby inhibitory interneurons to produce a network exhibiting the continuous attractor dynamics that generate individual grid cells?

While our model focuses on an already established cooperation between excitatory stellate cells, our results show that inhibitory interneurons can be easily recruited to refine the continuous attractor dynamics necessary to produce grid cells. In accordance with both the functional and structural development studies described in chapter 1, a stellate cell seeded network that uses simple plasticity

rules to generate continuous attractor behavior, exhibits both a rapid increase in inhibition driven by excitatory stellate cell activity and a rapid increase in refinement of the behavior of individual grid cells within the network, and could help to inform the actual development of grid cells during early postnatal life.

6.3 Future Work

To expand the utility of the computational model presented, several features could be added to the grid cell network itself or to the overall model structure in order to produce more precise, stable spatial representations. As described in Hardcastle et al and Musal et al, the incorporation of input from a network of border cells or place cells into the recurrent grid cell network reduces drift in the continuous attractor dynamics and yields more temporally stable activity. Including such a stabilizing input into the network could prevent drift in the single population network and induce reliability in the dynamics of the dual population model.

Another feature of the medial entorhinal cortex that could be incorporated into the model and explored is the presence of a theta modulation. Namely, the external input to the network could assume a theta modulated structure. With this alteration, the behavior of grid cells could be analyzed to observe the presence of phase precession as a temporal code. Simulations could also reveal if STDP learning rules in the dual population network model also refine towards continuous attractor dynamics given a theta modulated input.

Finally, to produce a complete developmental model of a grid cell network, mechanisms that use the coordination of clonally related stellate cells to generate a network with continuous attractor dynamics can be explored. If simple connectivity rules between excitatory cells are capable of producing the blueprint of a grid cell network, then the network could rely more on genetic underpinnings than extended activity-dependent experience to develop into a refined state.

References

[1] E. I. Moser, E. Kropff, and M.-B. Moser, "Place cells, grid cells, and the brain's spatial representation system," *Annual Review of Neuroscience*, vol. 31, pp. 69–89, 2008.

[2] T. Hafting, M. Fyhn, S. Molden, M.-B. Moser, and E. I. Moser, "Microstructure of a spatial map in the entorhinal cortex," *Nature*, vol. 436, pp. 801–806, 2005.

[3] C. N. Boccara, F. Sargolini, V. H. Thoresen, T. Solstad, M. P. Witter, E. I. Moser, and M.-B. Moser, "Grid cells in pre- and parasubiculum," *Nature Neuroscience*, vol. 13, pp. 987–994, 2010.

[4] C. W. Gatome, L. Slomianka, and I. Amrein, "Number estimates of neuronal phenotypes in layer ii of the medial entorhinal cortex of rat and mouse," *Neuroscience*, vol. 170, pp. 156–165, 2010.

[5] J. J. Couey, A. Witoelar, S.-J. Zhang, K. Zheng, J. Ye, B. Dunn, R. Czajkowski, M.-B. Moser, E. I. Moser, Y. Roudi, and M. P. Witter, "Recurrent inhibitory circuitry as a mechanism for grid formation," *Nature Neuroscience*, vol. 16, no. 3, pp. 318–324, 2013.

[6] E. C. Tolman, "Cognitive maps in rats and men," *The Psychological Review*, vol. 55, pp. 189–208, 1948.

[7] B. L. McNaughton, F. P. Battaglia, O. Jensen, E. I. Moser, and M.-B. Moser, "Path integration and the neural basis of the 'cognitive map'," *Nature Reviews Neuroscience*, vol. 7, pp. 663–678, 2006.

[8] D. Bush, B. Caswell, D. Manson, and N. Burgess, "Using grid cells for navigation," *Neuron*, vol. 87, pp. 507–520, 2015.

[9] J. O'Keefe and J. Dostrovsky, "The hippocampus as a spatial map. preliminay evidence from unit-activity in the freely moving rat." *Brain Res*, vol. 34, no. 1, pp. 171–175, 2009.

[10] J. O'Keefe, "Place units in the hippocampus of the freely moving rat," *Experimental Neurology*, vol. 51, pp. 78–109, 1976.

[11] J. O'Keefe and N. Burgess, "Dual phase and rate coding in hippocampal place cells: Theoretical significance and relationship to entorhinal grid cells," *Hippocampus*, vol. 15, no. 7, pp. 853–866, 2005.

[12] T. Bonnevie, B. Dunn, M. Fyhn, T. Hafting, D. Derdikman, J. L. Kubie, Y. Roudi, E. I. Moser, and M.-B. Moser, "Grid cells require excitatory drive from the hippocampus," *Nature Neuroscience*, vol. 16, no. 3, pp. 309–317, 2016.

[13] M. Moser, D. Rowland, and E. Moser, "Place cells, grid cells, and memory," *Cold Springs Harbor Perspectives Biology*, vol. 7, 2015.

[14] J. Taube and J. Bassett, "Persistent neural activity in head direction cells," *Cerebral Cortex*, vol. 13, pp. 1162–1172, 2003.

[15] J. Ranck, "Head direction cells in the deep layer of dorsal presubiculum in freely moving rats," *Society for Neuroscience Abstract*, 1984.

[16] J. S. Taube, R. U. Muller, and J. B. Ranck, "Head-direction cells recorded from the postsubiculum in freely moving rats. i. description and quantitative analysis," *The Journal of Neuroscience*, vol. 10, pp. 420–435, 1990.

[17] L. M. Giocomo, T. Stensola, T. Bonnevie, T. Van Cauter, M.-B. Moser, and E. I. Moser, "Topography of head direction cells in medial entorhinal cortex," *Current Biology*, vol. 24, pp. 252–262, 2014.

[18] L. Chen, L. Lin, E. Green, C. Barnes, and B. McNaughton, "Head-direction cells in the rat posterior cortex. i. anatomical distribution and behavioral modulation," *Exp. Brain Res.*, vol. 101, pp. 8–23, 1994.

[19] J. Taube, "Head direction cells recorded in the anterior thalamic nuclei of freely moving rats," *Journal of Neuroscience*, vol. 15, pp. 70–86, 1995.

[20] J. Cho and P. Sharp, "Head direction, place, and movement correlates for cells in the rat retrosplenial cortex," *Behavioral Neuroscience*, vol. 115, pp. 3–25, 2001.

[21] T. Solstad, C. N. Boccara, E. Kropff, M.-B. Moser, and E. I. Moser, "Representation of geometric borders in the entorhinal cortex," *Science*, vol. 322, pp. 1865–1868, 2008.

[22] E. Kropff, J. E. Carmichael, M.-B. Moser, and E. I. Moser, "Speed cells in the medial entorhinal cortex," *Nature*, vol. 523, pp. 419–424, 2015.

[23] R. F. Langston, J. A. Ainge, J. J. Couey, C. B. Canto, T. L. Bjerknes, M. P. Witter, E. I. Moser, and M.-B. Moser, "Development of the spatial representation system in the rat," *Science*, vol. 328, pp. 1576–1580, 2010.

[24] T. J. Wills, F. Cacucci, N. Burgess, and J. O'Keefe, "Development of the hippocampal cognitive map in preweanling rats," *Science*, vol. 328, pp. 1573–1576, 2010.

[25] T. J. Wills, C. Barry, and F. Cacucci, "The abrupt development of adult-like grid cell firing in the medial entorhinal cortex," *Front. Neural Circuits*, vol. 6, no. 21, 2012. [Online]. Available: doi:10.3389/fncir.2012.00021

[26] F. Donato, R. I. Jacobsen, M.-B. Moser, and E. I. Moser, "Stellate cells drive maturation of the entorhinal-hippocampal circuit," *Science*, 2017. [Online]. Available: DOI:10.1126/science.aai8178

[27] E. I. Moser, Y. Roudi, M. P. Witter, C. Kentros, T. Bonhoeffer, and M.-B. Moser, "Grid cells and cortical representation," *Nature Reviews Neuroscience*, vol. 15, pp. 466–481, 2014.

[28] M. Hasselmo, L. Giocomo, and E. A. Zilli, "Grid cell firing may arise from interference of theta frequency membrane potential oscillations in single neurons," *Hippocampus*, vol. 17, pp. 1252–1271, 2007.

[29] N. Burgess, C. Barry, and J. O'Keefe, "An oscillatory interference model of grid cell firing," *Hippocampus*, vol. 17, pp. 801–812, 2007.

[30] A. Guanella, D. Kiper, and P. Verschure, "A model of grid cells based on a twisted torus topology," *International Journal of Neural Systems*, vol. 17, pp. 231–240, 2007.

[31] Y. Burak and I. R. Fiete, "Accurate path integration in continuous attractor network models of grid cells," *PLOS Computational Biology*, vol. 5, no. 2, 2009.

[32] M. Yartsev, M. Witter, and N. Ulanovsky, "Grid cells without theta oscillations in the entorhinal cortex of bats," *Nature*, vol. 479, pp. 103–107, 2011.

[33] N. Killian, M. Jutras, and E. Buffalo, "A map of visual space in the primate entorhinal cortex," *Nature*, vol. 491, pp. 761–764, 2012.

[34] C. Domnisoru, A. Kinkhabwala, and D. Tank, "Membrane potential dynamics of grid cells," *Nature*, vol. 495, pp. 199–204, 2013.

[35] C. Schmidt-Hieber and M. Haeusser, "Cellular mechanisms of spatial navigation in the medial entorhinal cortex," *Nature Neuroscience*, vol. 16, pp. 325–331, 2013.

[36] H. Pastoll, L. Solanka, M. van Rossum, and M. Nolan, "Feedback inhibition enables theta-nested gamma oscillations and grid firing fields," *Neuron*, vol. 77, pp. 141–154, 2013.

[37] K. Yoon, M. A. Buice, B. Caswell, R. Hayman, N. Burgess, and I. R. Fiete, *Nature Neuroscience*, vol. 16, pp. 1077–1084, 2013.

[38] E. Kropff and A. Treves, "The emergence of grid cells: intelligent design or just adaptation?" *Hippocampus*, vol. 18, pp. 1256–1269, 2008.

[39] J. Widloski and I. R. Fiete, "A model of grid cell development through spatial exploration and spike time-dependent plasticity," *Neuron*, vol. 83, pp. 481–495, 2014.

[40] S. Song and L. Abbott, "Cortical development and remapping through spike timing-dependent plasticity," *Neuron*, vol. 32, pp. 339–350, 2001.

[41] J. R. Hinman, M. P. Brandon, J. R. Climer, G. W. Chapman, and M. E. Hasselmo, "Multiple running speed signal in medial entorhinal cortex," *Neuron*, vol. 91, pp. 666–679, 2016.

[42] D. Justus, D. Dalugge, S. Bothe, F. Fuhrmann, C. Hannes, H. Kaneko, D. Friedrichs, L. Sosulina, I. Schwarz, D. A. Elliot, S. Schoch, F. Bradke, M. K. Schwarz, and S. Remy, "Glutamatergic synaptic integration of locomotion speed via septoentorhinal projections," *Nature Neuroscience*, vol. 20, pp. 16–19, 2017.

[43] A. Turing, "The chemical basis of morphogenesis," *Philosophical Transactions of the Royal Society of London*, vol. 237, pp. 37–72, 1952.

[44] C. Buetfering, K. Allen, and H. Monyer, "Parvalbumin interneurons provide grid cell-driven recurrent inhibition in the medial entorhinal cortex," *Nature Neuroscience*, vol. 17, pp. 710–718, 2014.

[45] A. Dhillon and R. S. G. Jones, "Laminar differences in recurrent excitatory transmission in the rat entorhinal cortex in vitro," *Neuroscience*, vol. 99, no. 3, pp. 413–422, 2000.

[46] H. Dale, "Pharmacology and nerve-endings," *Proceedings of the Royal Society of Medicine*, vol. 28, pp. 319–330, 1934.

[47] J. S. Haas, T. Nowotny, and H. Abarbanel, "Spike-timing-dependent plasticity of inhibitory synapses in the entorhinal cortex," *Journal of Neurophysiology*, vol. 96, pp. 3305–3313, 2006. [Online]. Available: doi.10.1152/jn.00551.2006

[48] J.-t. Lu, C.-y. Li, J.-P. Zhao, M.-m. Poo, and X.-h. Zhang, "Spike-timing-dependent plasticity of neocortical excitatory synapses on inhibitory interneurons depends on target cell type," *Journal of Neuroscience*, vol. 36, pp. 9711–9720, 2007.

[49] E. Fino and L. Venance, "Spike-timing dependent plasticity in the striatum," *Frontiers in Synaptic Neuroscience*, vol. 2, 2010.

[50] S. Huang, R. Huganir, and A. Kirkwood, "Adrenergic gating of hebbian spike-timing-dependent plasticity in cortical interneurons," *Journal of Neuroscience*, vol. 32, pp. 13 171–13 178, 2013.

[51] D. Feldman, "The spike-timing dependence of plasticity," *Neuron*, vol. 75, pp. 556–571, 2012.

[52] F. Sargolini, M. Fyhn, T. Hafting, B. McNaughton, M. Witter, M. Moser, and E. Moser, "Conjunctive representation of position, direction, and velocity in entorhinal cortex," *Science*, vol. 312, pp. 758–762, 2006.

[53] K. Hardcastle, S. Ganguli, and L. Giocomo, "Environmental boundaries as an error correction mechanism for grid cells," *Neuron*, vol. 86, pp. 827–839, 2015.

[54] M. Mulas, N. Waniek, and J. Conradt, "Hebbian plasticity realigns grid cell activity with external sensory cues in continuous attractor models," *Frontiers in Computational Neuroscience*, 2016. [Online]. Available: doi:10.3389/fncom.2016.00013

[55] Y. Li, H. Lu, P.-l. Cheng, S. Ge, H. Xu, S.-H. Shi, and D. Yang, "Clonally related visual cortical neurons show similar stimulus feature selectivity," *Nature*, vol. 486, pp. 118–121, 2012.

[56] Y. Yu, R. Bultje, X. Wand, and S. Shi, "Specific synapses develop preferentially amond sister excitatory neurons in the neocortex," *Nature*, vol. 458, pp. 501–504, 2009.

[57] A. Alonso and R. Klink, "Differential electroresponsiveness of stellate and pyramidal-like cells of medial entorhinal cortex layer ii," *Journal of Neurophysiology*, vol. 70, pp. 128–143, 1993.

Appendix A

Overview of Scripts

Rate-Based Grid Cell Network

1. defrateGCN.py
2. rateparameters.py
3. runratesimulation.py

Single Population Spiking Grid Cell Network

1. defspikingGCN.py
2. spikingparameters.py
3. runspikingsimulation.py

Dual Population Spiking Grid Cell Network

1. defspikingEIGCN.py
2. spikingEIparameters.py
3. runspikingEIsimulation.py

Dual Population Spiking Grid Cell Network with STDP

1. defspikingEIGCN_STDP.py
2. spikingEIGCN_STDPparameters.py
3. runspikingEIGCN_STDPsimulation.py

Supporting Scripts

1. gridnessscore.py
2. randomwalk.py
3. spikeoverlay.py
4. spikinganimation.py
5. neuronalactivationanimation.py

Code Availability

```
All code is available online at:
\href{https://www.tug.org/texlive/}{https://www.tug.org/texlive/}
```

Appendix B

Calculation of Gridness Scores

The analysis of grid cell scores was completed in accordance with the methods in Sargolini et al [52].

The average firing rate for all locations within the arena is calculated by,

$$\lambda(x) = \frac{\sum_{i=1}^{n} g(\frac{s_i - x}{h})}{\int_0^T g(\frac{y(t)-x}{h})dt} \tag{B.1}$$

where g is a smoothing kernel and h is a smoothing factor. The upper bound of summation, n, is the number of total spikes occurring throughout motion. The location of the spike is given by s_i, where *y(t)* indicates the location of the agent at time t of the spike. The summation in the denominator runs over the full recording time, [0,T].

The above formula is used to determine the spatial autocorrelation below, where $\lambda_1(x,y)$ and $\lambda_2(x,y)$ identify the average firing rate of cells *1* and *2*, respecitvely, at location *(x,y)*. The summation is completed over all positions τ_x and τ_y.

$$r(\tau_x, \tau_y) = \frac{n\sum\lambda_1(x,y)\lambda_2(x-\tau_x, y-\tau_y) - \sum\lambda_1(x,y)\sum\lambda_2(x-\tau_x, y-\tau_y)}{\sqrt{n\sum\lambda_1(x,y)^2(\sum\lambda_1(x,y))^2}\sqrt{n\sum\lambda_2(x-\tau_x, y-\tau_y)^2(\sum\lambda_2(x-\tau_x, y-\tau_y))^2}} \tag{B.2}$$

The gridness score is then calculated by rotating the autocorrelation map formed with equation B.2. The map is rotated by 6° increments, where at each step, the correlation is computed. From this set of correlations, the maximum value between autocorrelations at rotation angles 30°, 90°, and 150° is subtracted from the minimum value between autocorrelations at rotation angles 60° and 120°.